Synoptic and Mesoscale Environment of Convection during the North American Monsoon across Central and Southern Arizona

LEE B. CARLAW[a]

National Weather Service Forecast Office, Tucson, Arizona

ARIEL E. COHEN AND JARET W. ROGERS

NOAA/NWS/NCEP/Storm Prediction Center, Norman, Oklahoma

(Manuscript received 5 August 2015, in final form 24 September 2016)

ABSTRACT

This paper comprehensively analyzes the synoptic and mesoscale environment associated with North American monsoon–related thunderstorms affecting central and southern Arizona. Analyses of thunderstorm environments are presented using reanalysis data, severe thunderstorm reports, and cloud-to-ground lightning information from 2003 to 2013, which serves as a springboard for lightning-prediction models provided in a companion paper. Spatial and temporal analyses of lightning strikes indicate thunderstorm frequencies maximize between 2100 and 0000 UTC, when the greatest frequencies are concentrated over higher terrain. Severe thunderstorm reports typically occur later in the day (between 2300 and 0100 UTC), while reports are maximized in the Tucson and Phoenix metropolitan areas. Composite analyses of the synoptic-scale patterns associated with severe thunderstorm days and nonthunderstorm days during the summer using the North American Regional Reanalysis dataset are presented. Severe thunderstorm cases tend to be associated with a stronger midlevel anticyclone and deep-layer moisture over portions of the southwestern United States. By September, severe weather patterns tend to associate with a midlevel trough along the Pacific coast. Specific parameters associated with severe thunderstorms are analyzed across the Tucson and Phoenix areas, where severe weather reporting is more consistent. Greater convective available potential energy, low-level lapse rates, and downdraft convective available potential energy are associated with severe thunderstorm (especially severe wind) environments compared to those with nonsevere thunderstorms, while stronger effective bulk wind differences (at least 15–20 kt, where 1 kt = 0.51 m s^{-1}) can be used to distinguish severe hail environments.

1. Introduction

a. The North American monsoon

During the early summer, the upper-air pattern across the Southwest undergoes a substantial evolution as mid- and upper-level winds switch from westerly to easterly or southeasterly. Bryson and Lowry (1955) were among the first to recognize that this was a result of the poleward movement and westward expansion of the Bermuda high during the end of June. Coincident with this alteration to the flow pattern is typically a marked increase in moisture and convection over northern Mexico and much of the Southwest (Bryson and Lowry 1955; Sellers and Hill 1974; Douglas et al. 1993). This surge of seasonal moisture and subsequent increase in precipitation has been called, most recently, the North American monsoon, but has been referred to by a number of different names, including the Mexican or Arizona monsoon (Adams and Comrie 1997).

The initial literature on the Arizona summer monsoon suggested that the source region for this moisture could be traced back to the Gulf of Mexico, since the wind shift in the mid- and upper levels would facilitate the advection of tropical moisture from the Gulf of Mexico into Arizona and northern Mexico (Bryson and Lowry 1955; Green and Sellers 1964; Sellers and Hill 1974). However, Reitan (1957) found that a large percentage of the precipitable water (PW) during July in the Phoenix, Arizona, area was confined below the 800-mb (1 mb = 1 hPa) level, more or less ruling out the Gulf of Mexico as the primary source region given this moisture

[a] Current affiliation: National Weather Service Forecast Office, Fort Worth, Texas.

Corresponding author e-mail: Lee Carlaw, lee.carlaw@noaa.gov

DOI: 10.1175/WAF-D-15-0098.1

must ascend to elevations in excess of 5000 m over parts of Mexico before reaching Arizona. More recent work has shown that air originating over the Gulf of California is the primary source of the low-level moisture over Arizona, which is advected northward by thermally driven pressure gradients along the Baja coast during the summer (Rasmusson 1967; Hales 1974; Tang and Reiter 1984; Maddox et al. 1995). Carleton (1986) suggests that in addition to the low-level moisture originating from the Gulf of California, the moisture noted in the mid- and upper levels could be traced back to the Gulf of Mexico.

During a typical year, portions of central and southern Arizona experience up to 80 thunderstorm days, a vast majority of which are realized during the 3-month period from July to September (Shoemaker and Davis 2008). Thus, during the peak of the summer monsoon, thunderstorms are a nearly daily occurrence across parts of the region. Thunderstorms during the summer monsoon produce a wide variety of hazardous weather, from damaging wind gusts, hail, dust storms, and flash flooding caused by torrential rainfall, to an occasional tornado (Glueck 1997).

b. *Purpose of this work*

While the literature focusing on the North American monsoon is vast, spanning more than half a century [see Adams and Comrie (1997) for a comprehensive overview of the previous research], comparatively little work exists on central and southern Arizona severe weather climatology during the summer monsoon, and even less applies thermodynamic and kinematic parameters for use in an operational meteorology environment for both general thunderstorms and severe thunderstorms. Shoemaker and Davis (2008) compiled a summary of hazardous-weather events across Arizona using nearly five decades' worth of meteorological data, but this is one of the few studies to our knowledge that focuses on detailed spatiotemporal distributions of severe weather reports during the North American monsoon.[1] McCollum (1993) and Maddox et al. (1995) used several thunderstorm events to composite the synoptic-scale patterns and conditions associated with severe weather across Arizona during the summer monsoon to provide operational forecasters with a basis for pattern recognition to improve forecasting techniques.

The purpose of this paper is multifold. First, we use lightning data from the National Lightning Detection Network (NLDN; Cummins and Murphy 2009) and severe thunderstorm reports from the National Centers for Environmental Information's (NCEI) *Storm Data* publication with the goal of expanding upon the previous work by Shoemaker and Davis (2008) to develop a climatology of thunderstorm and severe weather events across central and southern Arizona during the summer monsoon. We additionally investigate thermodynamic and kinematic parameters associated with monsoonal convection in Arizona by exploring the spatial variability in the frequencies of these phenomena within the most convectively active periods of the diurnal cycle and develop distributions of thermodynamic and kinematic variables associated with severe thunderstorm reports. Storm report and NLDN data were used in conjunction with the National Centers for Environmental Prediction (NCEP) North American Regional Reanalysis (NARR) to illustrate the synoptic-scale patterns and distribution of thermodynamic variables associated with severe thunderstorm and nonsevere thunderstorm days in central and southern Arizona, expanding upon the work of McCollum (1993) and Maddox et al. (1995).

A companion paper (Rogers et al. 2017) focuses on the direct applications of this research to operational meteorology. In particular, we identify several moisture and instability variables using sounding data from Phoenix and Tucson, Arizona, and regularly updated gridded datasets, featuring some correlation to domain-wide lightning. The variables from the sounding data were used to develop a multiple-linear regression model to predict total lightning over a 24-h period using sounding data as input across the region. Additionally, a logistic regression model was developed using data from the gridded datasets to create 3-h probabilistic forecasts of lightning occurrences on a 40-km-grid basis.

To the best of our knowledge, this is the first set of publications to 1) examine the climatology of central and southern Arizona convection during the summer monsoon with the Surface Objective Analysis (SFCOA) dataset developed by the Storm Prediction Center (SPC; Bothwell et al. 2002) and the NARR reanalysis, 2) perform a comprehensive analysis of the convective environment associated with central and southern Arizona thunderstorms, and 3) develop logistic-regression

[1] Prior to 2008, the operational criteria for defining the onset of the summer monsoon in southeast Arizona was the first in a 3-day period in which dewpoint temperatures averaged 54°F or higher at the Tucson International Airport (55°F at Phoenix Sky Harbor International Airport to account for the lower elevation). Based on this definition, the summer monsoon typically ran from 5 July through 15 September (Glueck 1997). However, after 2008, strict dates were used to delineate the beginning and end of the Arizona summer monsoon based on the climatology of precipitation, much like the method employed by the National Hurricane Center in defining the hurricane season. These dates are 15 June through 30 September, which has motivated our decision to break up our analyses and results into intervals spanning June–September in this work.

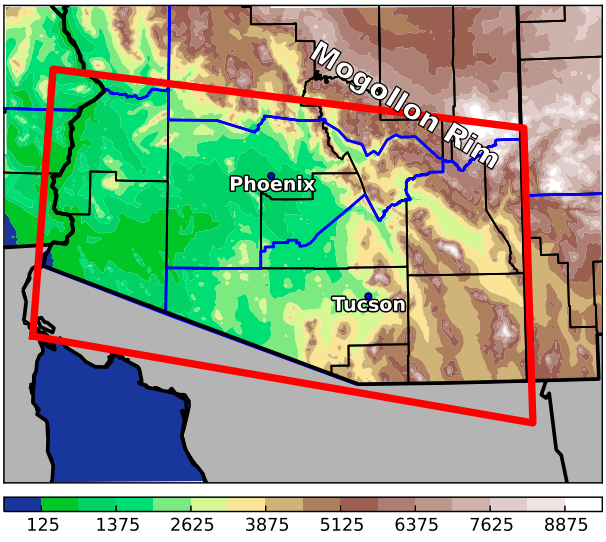

FIG. 1. Domain used in this study (red outline) along with the central and southern AZ CWAs (blue outline). Counties are shown as black lines, and terrain is shown in the background shading (ft).

models for thunderstorm probabilities with clear utility to the operational forecaster.

2. Dataset information

The domain for this study, which includes the Arizona counties of the Phoenix and Tucson National Weather Service (NWS) County Warning Areas (CWAs), is shown in Fig. 1. The environmental parameters examined in this study span an 11-yr period, from 2003 to 2013, and are obtained from the SFCOA dataset.

The SFCOA system merges an objective analysis performed on surface thermodynamic observations using the 0-h Rapid Refresh (RAP) as background with RAP data aloft. This creates a best guess of the atmospheric state at 40-km grid length upon which sounding analysis routines, based on those developed by Hart and Korotky (1991), are performed. For more information on the SFCOA procedure, the interested reader is directed to Bothwell et al. (2002, 2014).

Storm reports for severe thunderstorm wind, hail, and tornadoes are obtained via the NCEI *Storm Data* publication, which consists of severe thunderstorm reports collected by NWS offices. Lightning data from the NLDN consists of the number of cloud-to-ground (CG) strikes recorded in each 40-km grid box. Finally, the data used in the composite-analysis section of this paper are obtained from the NARR (Mesinger et al. 2006), which is an eight-times-daily dataset at approximately 32-km horizontal grid spacing on 29 pressure levels.

3. Climatology of central and southern Arizona lightning and severe reports

a. *Lightning climatology*

Figure 2 displays the domain-average number of CG lightning strikes every hour. A diurnal trend is noted, with a minimum in thunderstorm activity between 1100 and 1600 UTC followed by an increase in activity during the early afternoon, peaking for all months between 2100 and 0000 UTC. These results agree with previous work by King and Balling (1994), Rasmusson (1971),

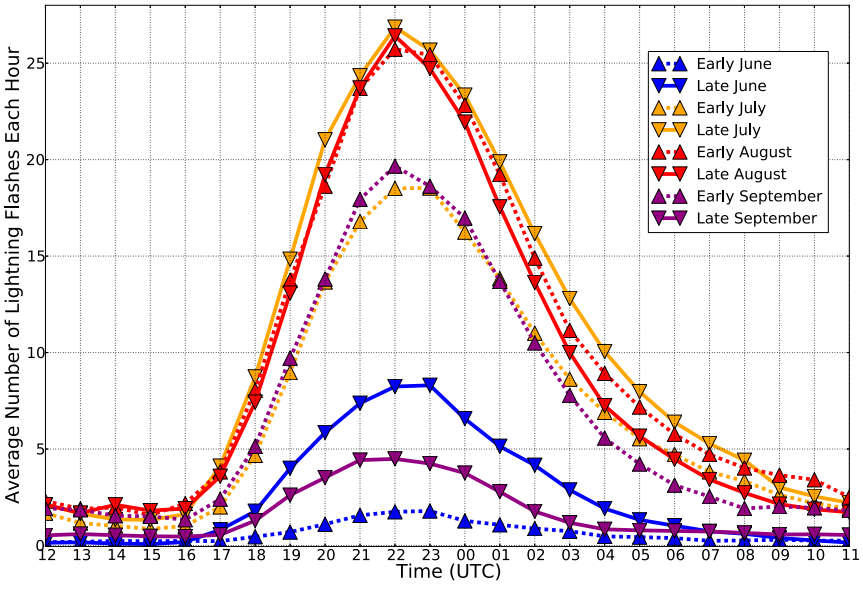

FIG. 2. Hourly average number of CG lightning strikes across the domain grouped into half-month periods. Nomenclature for months follows that outlined in Table 1.

TABLE 1. Month-portion nomenclature.

Portion of month	Dates
Early Jun	1–15 Jun
Late Jun	16–30 Jun
Early Jul	1–15 Jul
Late Jul	16–31 Jul
Early Aug	1–15 Aug
Late Aug	16–31 Aug
Early Sep	1–15 Sep
Late Sep	16–30 Sep

and Reap (1986), all of whom found thunderstorm occurrences peaked between 3 and 5 h after local noon (2200–0000 UTC). This propensity for thunderstorms to develop during the midafternoon is indicative of the strong reliance of thunderstorm initiation on terrain-induced circulations (e.g., Doran and Zhong 1994; Bossert and Cotton 1994) during the period of peak heating in the absence of synoptic-scale forcing mechanisms, which typifies the atmospheric conditions present during a typical summer monsoon day (Douglas et al. 1993). During the evening, the lack of insolation leads to a nocturnally stabilizing boundary layer; one that is more hostile to the maintenance and/or development of thunderstorms.

A clear signal in the lightning data reveals the typical onset of the more convectively active period during the beginning of the summer monsoon, realized by the increase in cloud-to-ground strike occurrences between early June and early July (see Table 1 for an explanation of the half-month nomenclature used throughout the rest of these papers). The most convectively active periods of the summer monsoon are from late July through late August, with lightning-strike rates peaking during the afternoons in late July at nearly 28 strikes per hour over the domain. September is typically the transition period out of the summer monsoon, when daily lightning-strike rates decrease substantially.

To examine the spatial variability of lightning within the most convectively active period of the diurnal cycle, we constructed plan-view plots of lightning frequency by recording the number of CG lightning strikes every hour within each 40-km grid box across the domain. Then, the number of hours featuring at least one lightning strike was compared to the total number of hours of record to derive a lightning-hour frequency for each grid box. A similar methodology was employed to analyze the spatial distribution of severe reports in section 3b. To aid in the visualization of these plots, the data were linearly interpolated to a resolution of approximately 10 km.

The particular spatial distribution of lightning occurrence throughout the warm season is illustrated in Fig. 3, which highlights the proportion of hours during which lightning occurred within each partial-month period in the late afternoon. The greatest lightning-hour frequencies are apparent along portions of the Mogollon Rim (see Fig. 1) southward across the higher terrain of southeastern Arizona and adjacent state of Sonora in Mexico during July and August. During these periods, the greatest frequencies are concentrated along the

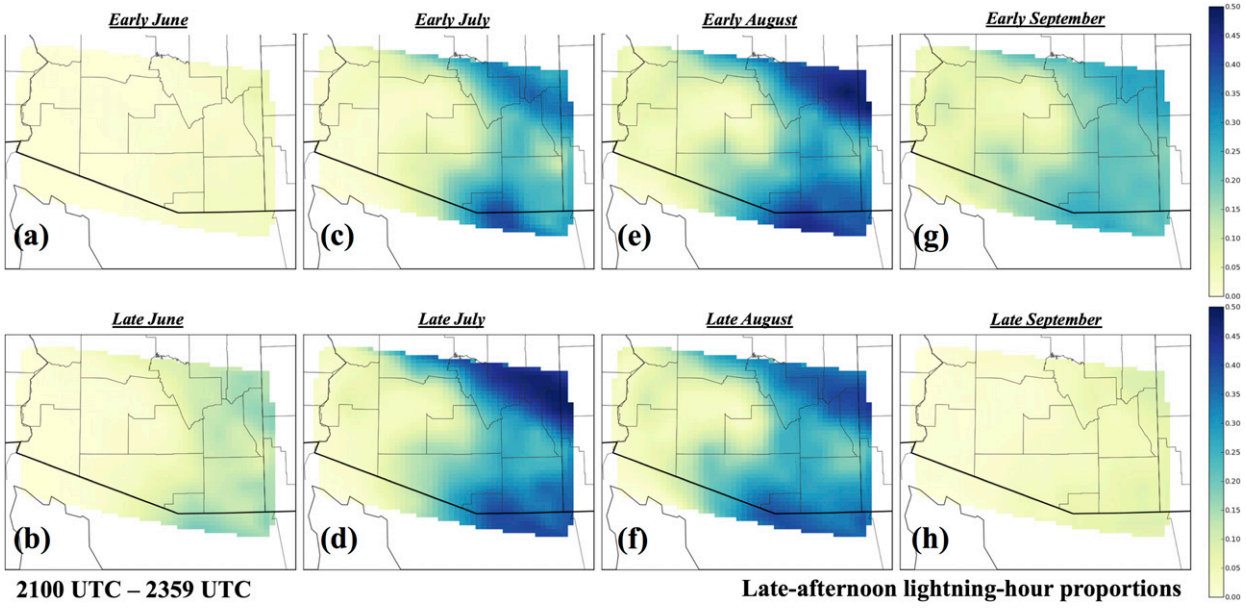

FIG. 3. Spatial distributions of proportion of hours during which lightning (lightning hours) occurred in the late afternoon (2100–2359 UTC) across the domain, separated by partial-month periods with nomenclature following that described in Table 1.

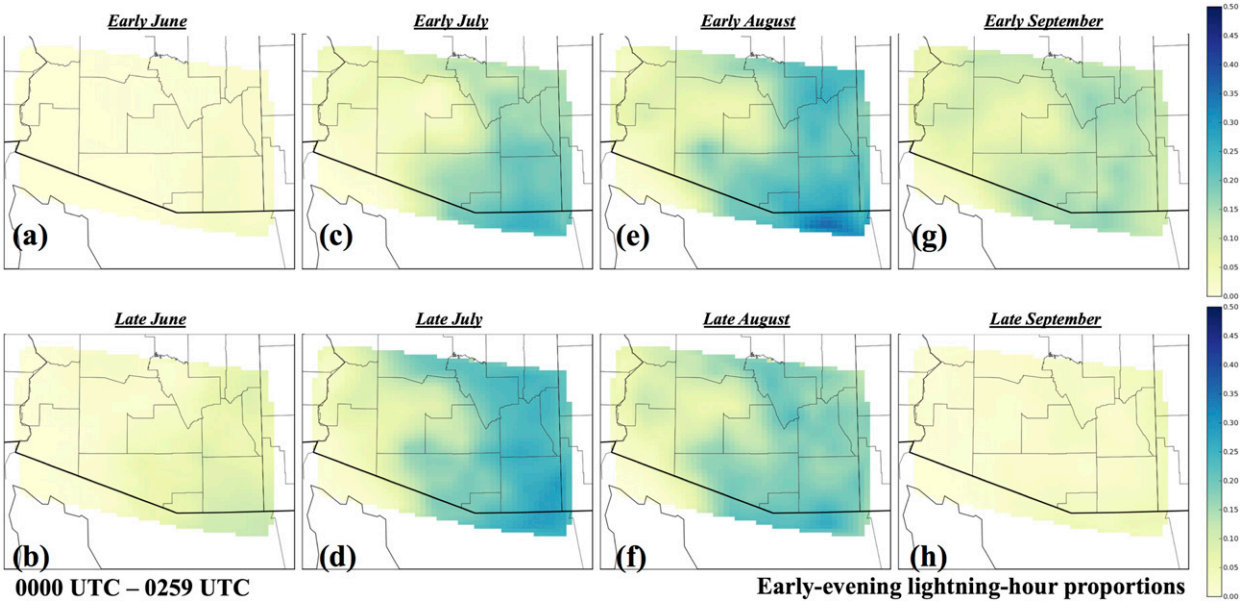

FIG. 4. As in Fig. 3, but during the early evening (0000–0259 UTC).

highest terrain, consistent with the notion that terrain-driven mesoscale and microscale circulations play a substantial role in the development of afternoon thunderstorms (e.g., Toth and Johnson 1985; Lopez and Holle 1986). An abrupt increase in late-afternoon lightning frequency is apparent from late June to early July, with a strong decreasing trend during September.

While the greatest lightning-hour frequencies during the late afternoon spatially coincide with the higher terrain, comparison of Fig. 3 to Fig. 4 suggests that such frequencies dampen substantially from late afternoon to early evening. Lower frequencies are apparent over the higher terrain across the eastern and far northern portions of the domain during the early evening. However, low frequencies begin to spread west of the highest southeastern Arizona terrain toward the desert floor of central, south-central, and southwestern Arizona. These areas experience near-zero lightning frequencies during the late-afternoon period.

Many of the aforementioned findings regarding lightning-hour frequency are largely consistent with work presented by King and Balling (1994), who identify spatial variability in peak lightning occurrences. The present study augments their work by providing a higher-resolution analysis (both seasonally and diurnally) of lightning data. The influence of terrain-related convection in maximizing lightning-hour frequencies in proximity to higher elevations, including the Mogollon Rim, is evident in both studies.

Increases in lightning frequency over the lower elevations following the peak of the diurnal heating cycle (cf. Fig. 4 to Fig. 3) have been the focus of other studies, which propose possible explanations. For example, midlevel transport of relatively cooler air emanating from earlier convection over the Mogollon Rim could explain destabilization, descending levels of free convection, and eventual postafternoon convection away from the higher terrain (Hales 1977). Maddox et al. (1991) suggest that terrain-descending outflow may encourage the spread of convection from the higher elevations to the lower elevations.

b. *Severe report climatology*

As noted by Shoemaker and Davis (2008), the low population density across our domain has likely resulted in numerous severe occurrences going unreported outside of urban areas. This population bias is evident in Fig. 5, which clearly shows disproportionate severe thunderstorm reports emanating from the higher-population Tucson and Phoenix areas than elsewhere across the domain during the entire record of analysis. Total severe thunderstorm counts and their corresponding deviations from the domain-wide median are maximized at metro-area-corresponding grid boxes. As a result, we stress that the severe-report climatology and subsequent spatial and environmental analyses only represent a subset of all severe-weather-producing thunderstorm events across the domain.

Figure 6 shows the domain-wide distribution of severe thunderstorm wind, hail, and tornado reports grouped by half-month interval. Significant wind [at least $33.4\,\mathrm{m\,s^{-1}}$ (65 kt; where $1\,\mathrm{kt} = 0.51\,\mathrm{m\,s^{-1}}$)] and hail [at

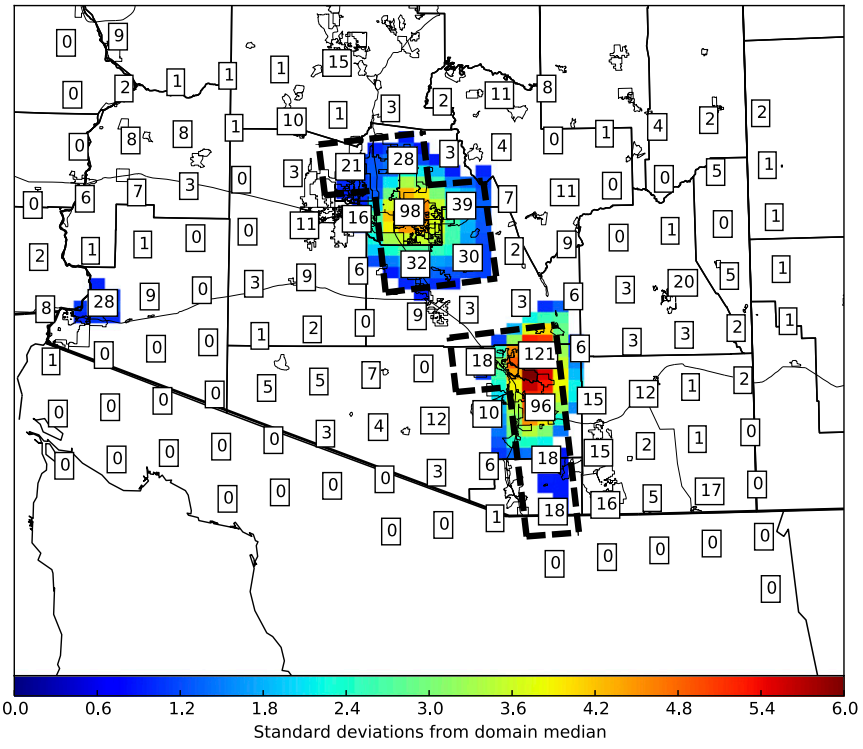

FIG. 5. Total number of severe thunderstorm reports that occurred in each grid box across the domain from 2003 to 2013 (listed numerically), and number of standard deviations (computed among all grid boxes) the total is away from the domain-wide median of two reports (background image is color filled, with values less than 1 not displayed). Black underlay indicates geographic boundaries (thickest for country boundary, thinnest for city outlines, and middle thickness for county and state outline). Overlaying dashed segments represent the bounding regions contributing to the ''urban domain'' covering the Tucson and Phoenix areas. Domain-wide median is 2 reports and standard deviation is 16 reports.

least 5.1 cm (2 in.)] reports are also displayed as hatched areas. The vast majority of severe reports are from thunderstorm winds, most of which occur between early July and early September. Winds tend to dominate the severe reports in association with the typical pulse-type convective mode owing to the generally weak synoptic-scale flow present during the summer monsoon (Douglas et al. 1993), along with deep, inverted-V boundary layer thermodynamic profiles (Maddox et al. 1995) supporting the formation of microbursts. This is particularly true during the early months of the summer monsoon when a paucity of moisture typically leads to very deep, dry subcloud layers, facilitating the evaporation of precipitation as it descends out of the base of the thunderstorm and the subsequent acceleration of the evaporatively cooled air (Vasiloff and Howard 2009).

Severe hail tends to be a rare occurrence, mainly because of the presence of very high freezing levels leading to considerable subcloud melting and sublimation (Shoemaker and Davis 2008), as well as an infrequent occurrence of supercells (Smith et al. 2013). A total of nine tornadoes were reported in the domain between 2003 and 2013. Tornadoes, while relatively scarce, do occur at a rate of about four per year (January–December) in Arizona, with most occurring outside of our analysis domain toward the high plateau north of the Mogollon Rim; however, this period falls outside of the summer monsoon (see Figs. 5 and 8 in Shoemaker and Davis 2008).

The temporal distribution of severe reports (all types) is shown in Fig. 7, in a similar manner to the lightning climatology displayed earlier (cf. Fig. 2). However, rather than display an average hourly severe report count, we show the number of days in which a severe report occurred within the analysis domain, broken down by hour. This method alleviates some of the analysis issues associated with severe reports tending to group together around a particular storm. Overall, the severe reports tend to occur later during the day, generally between 2300 and 0100 UTC, compared with the primary lightning maxima.

An increase in severe reports is noted between late June and early July, with the maximum number of

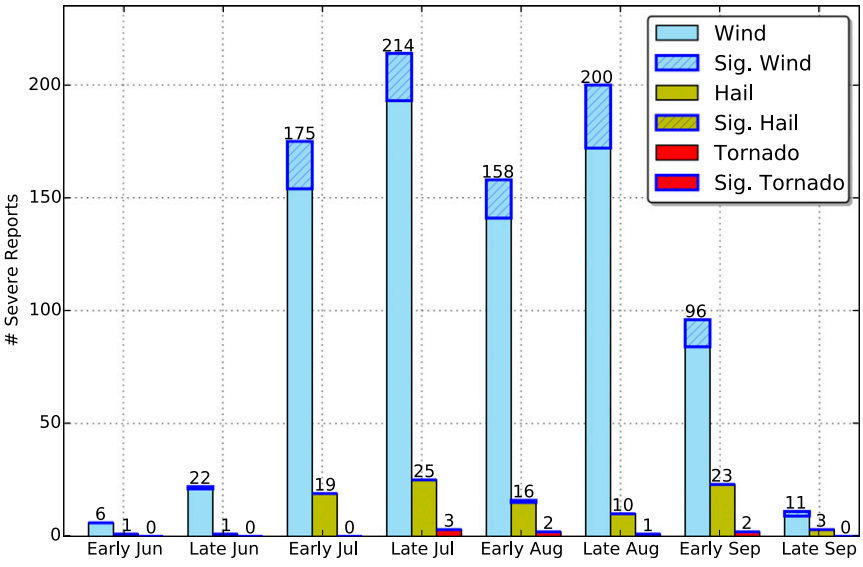

FIG. 6. Total number of severe reports (2003–13) for wind (blue shades), hail (yellow shades), and tornadoes (red shades) grouped into half-month intervals. Hatched areas represent significant wind (winds > 65 kt) and significant hail (hail > 2 in. in diameter) reports. There were no significant tornado reports in this dataset.

reports occurring a few weeks later during late July. During this peak period, a severe report is received within the domain on nearly 25% (38) of the days between 0000 and 0059 UTC. Severe reports during August remain near the levels observed during early July, with a precipitous decrease by late September. As seen previously in Fig. 6, a slight decrease in the number of severe thunderstorm reports is noted during early August, compared with the values observed for the last half of the month.

As may be expected for a region with low-population density outside of urban areas, spatial distributions of hourly severe thunderstorm frequencies do not strongly mirror those associated with lightning. There is a very clear tendency for the highest severe thunderstorm days to cluster around the Tucson and Phoenix metropolitan

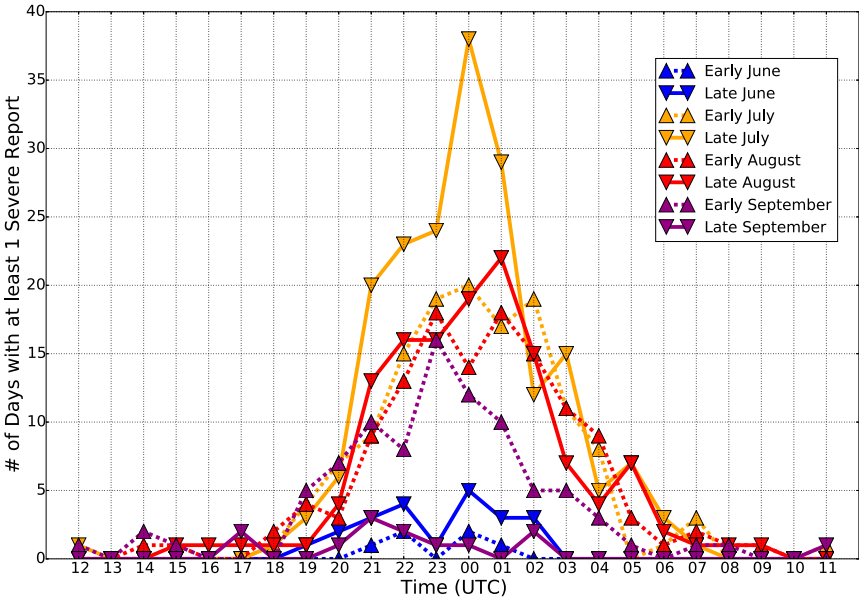

FIG. 7. Number of days with at least one severe report across the domain by hour grouped into half-month periods.

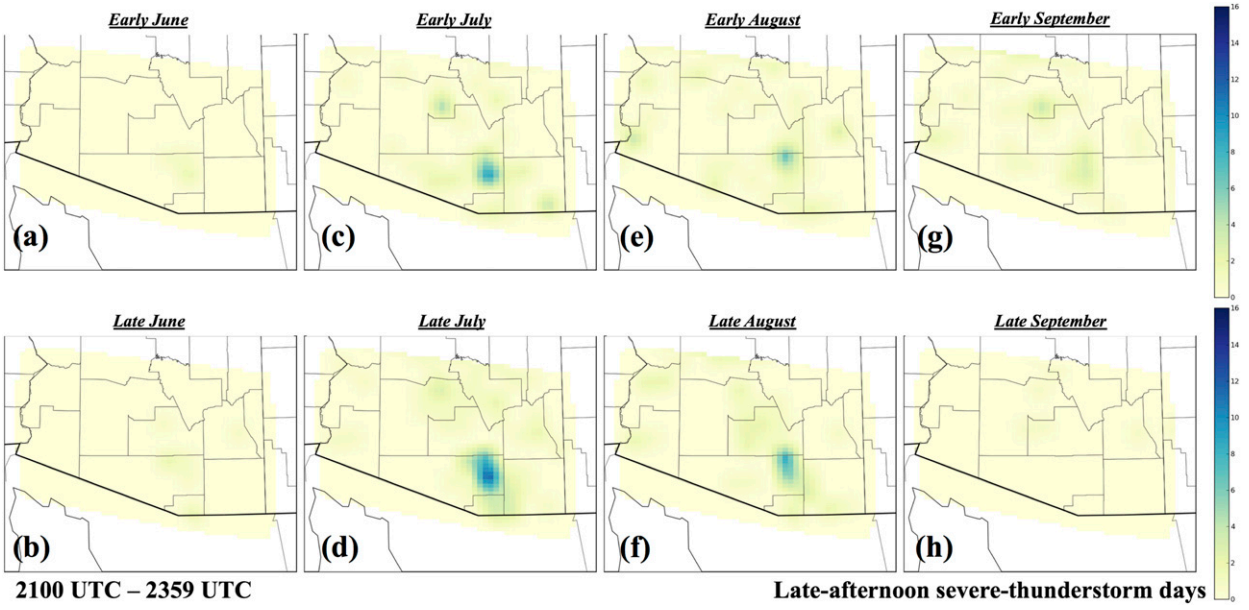

FIG. 8. Number of days with a severe report in the given half-month block during the late afternoon (2100–2359 UTC).

areas. July and August feature the most frequent occurrences of severe thunderstorms in the Tucson area, with a general lower occurrence (albeit higher than in nonurban areas) in Phoenix during these months (Figs. 8 and 9) except in late August. Comparison of Fig. 9 with Fig. 8 shows a general tendency for a higher number of severe thunderstorm days to exist in the Phoenix area during the early evening than late afternoon, which is consistent with the direction of convection-steering flow possessing some east-to-west component.

4. Composite analyses

a. Methodology

In this section, we investigate the synoptic patterns associated with severe thunderstorm events, defined as days with at least one severe report (which we refer to as ''severe event'' cases). Because the upper-air pattern associated with severe events tends to stagnate during the height of the summer monsoon (not shown), we separate our analyses into three periods to capture the most atmospheric variability, in addition to providing concise results. These periods are defined as 1 June–10 July (first third), 11 July–20 August (second third), and 21 August–30 September (final third). Thus, rather than attempting to identify large-scale pattern archetypes driving severe events as in McCollum (1993) and Maddox et al. (1995), we instead focus on the typical progression of synoptic-scale features through the summer monsoon. In addition, we make use of 1) all severe weather days (365) during the 2003–13 period of record to construct our analyses, in order to build on the analyses presented in Maddox et al. (1995), which used a set of 27 days of severe reports, and 2) the higher-resolution NARR reanalysis dataset.

Here, we composite 500-mb geopotential heights, PW, 500-mb temperatures, and 700-mb specific humidity on days with at least one severe report in our analysis domain (Fig. 1). These parameters were chosen based on the observation that they are among those typically employed by operational meteorologists to provide a basic overview of the atmospheric potential for thunderstorms during the summer monsoon and are easily accessible from operational workstations. Additionally, the inclusion of 700-mb specific humidity provides a metric for diagnosing the vertical distribution of moisture up to, near, or just below the convective cloud base. Finally, we display differences between the composite means of the severe cases and the corresponding cases in which no lightning strikes were recorded in the analysis domain in order to provide some contextualization for the presented severe patterns. We reiterate that the database of severe weather from NCEI storm data only represents a subset of all severe occurrences across our domain as a result of the large population bias present in central and southern Arizona.

b. Results

The composite analysis for severe days during the first third of the summer monsoon (1 June–10 July) is shown in Fig. 10. The severe weather synoptic-scale pattern is characterized by a 500-mb ridge centered roughly between the boot heel of New Mexico and the Four

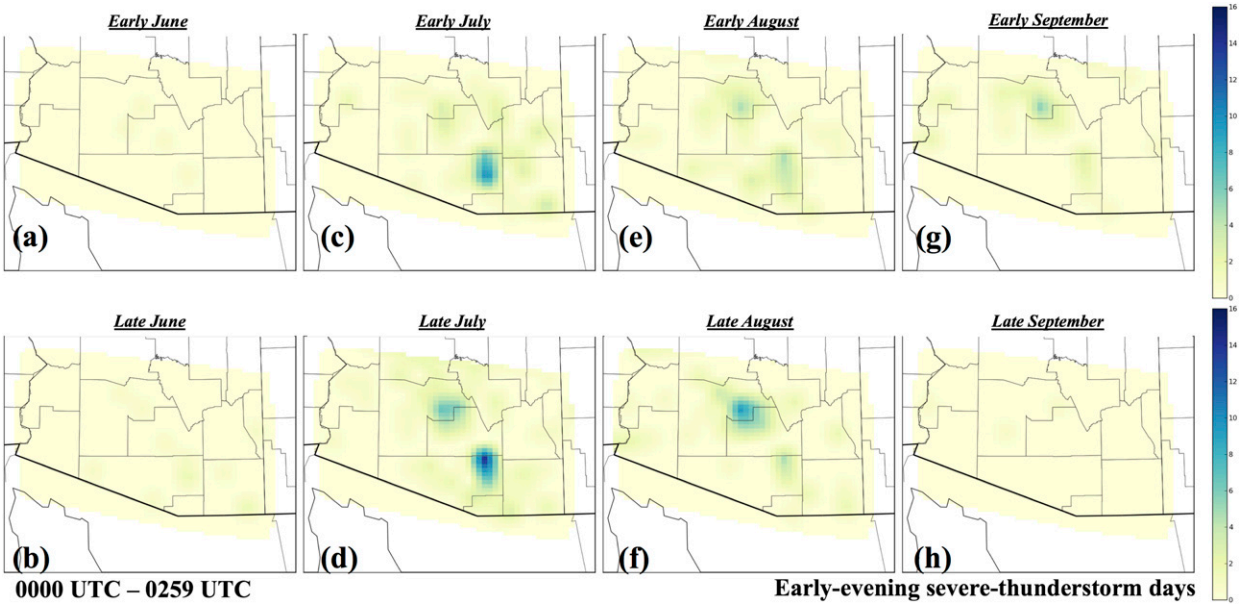

FIG. 9. As in Fig. 8, but during the early evening (0000–0259 UTC).

Corners region (Fig. 10a) along with PW values of 25–30 mm across southern Arizona (Fig. 10b). This moisture profile extends up to 700 mb, with specific humidity values near 6 g kg^{-1} across much of central and southern Arizona (Fig. 10d). Based on the shaded difference fields, it can be inferred that the no-thunder cases are dominated by generally west-to-east zonal flow in the midlevels and considerably drier moisture profiles, with PW and 700-mb specific humidity values effectively halved from the severe-case counterpart.

During the subsequent third of the summer monsoon (11 July–20 August), which encompasses the climatologically most active convective period across the domain (cf. Figs. 2 and 7), the 500-mb high in the severe cases

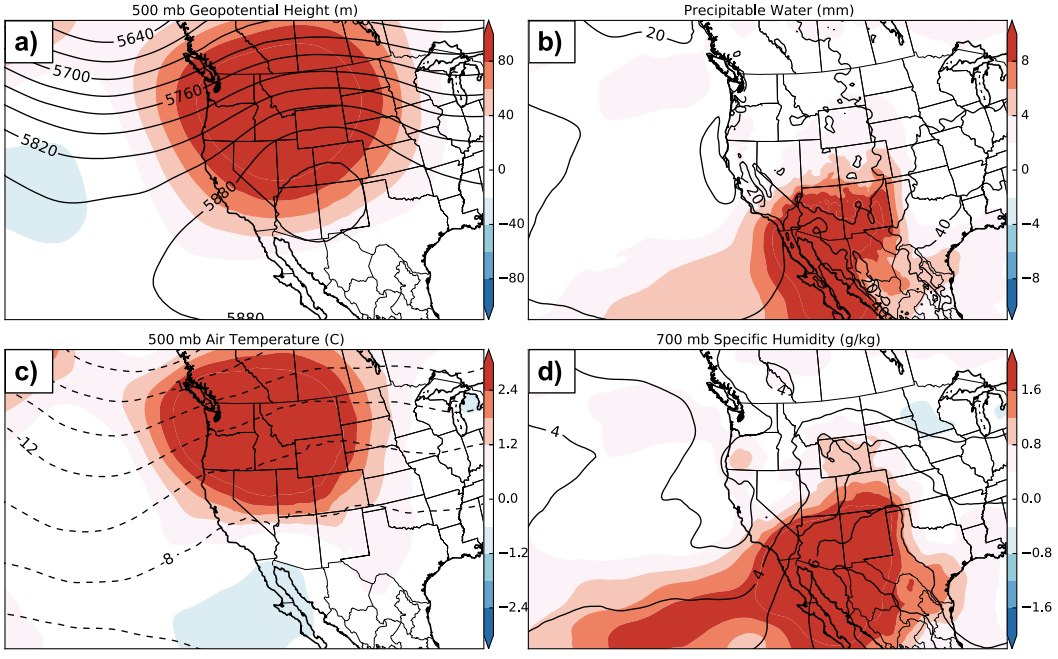

FIG. 10. Composite (contours) and differences from no-thunder days (shades) plots of (a) 500-mb geopotential height (m), (b) PW (mm), (c) 500-mb air temperature (°C), and (d) 700-mb specific humidity (g kg^{-1}) for severe weather days during 1 Jun–20 Jul. The number of days incorporated in the composite plot is $N = 66$.

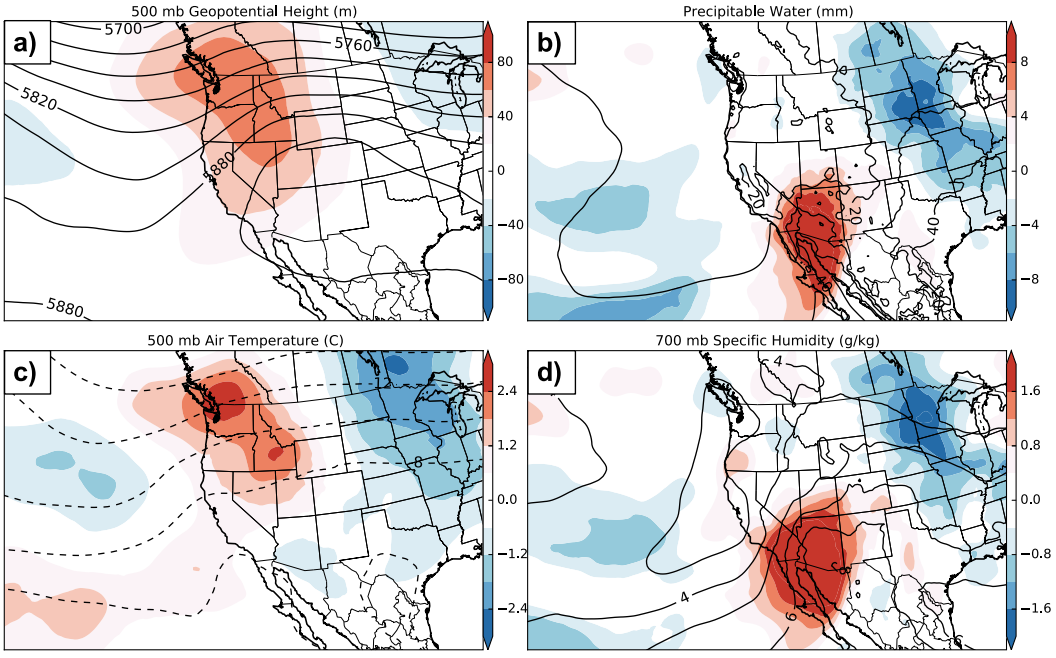

FIG. 11. As in Fig. 10, but for 21 Jul–10 Aug, with $N = 197$.

expands farther to the north, with the primary ridge axis extending into Alberta and British Columbia in Canada (Fig. 11a). As the midlevel high expands to the north, the 500-mb temperatures fall slightly compared with the no-thunder cases (Fig. 11c), while both of the moisture variables reach their greatest values attained during the summer monsoon. PW values increase to over 30 mm over most of the Tucson and Phoenix CWAs, while values of 7 g kg^{-1} of 700-mb specific humidity straddle the Sierra Madre Occidental in Mexico and extend into northern Arizona and New Mexico (Figs. 11b,d). This pattern qualitatively resembles the type I severe weather pattern identified by Maddox et al. (1995). This setup is characterized by a northwestward shift of the subtropical ridge into northern Oklahoma and the Four Corners region, along with large positive moisture departures across the Southwest (see Figs. 3 and 4 in Maddox et al. 1995).

The composite analysis of severe days in the final third period (21 August–30 September) reveals the subtle influence of more West Coast troughing compared with the previous two periods as the midlevel high moves southward and flattens (Fig. 12a). In these severe cases, this increasingly southwesterly flow still maintains a relatively deep layer of increased moisture across Arizona, as evidenced by 700-mb specific humidity values falling only slightly from the previous period, with indications of a subtropical moisture connection to the south and west (Fig. 12d). The no-thunder cases, as inferred from the color fills, are dominated by a suppressed midlevel high, as well as generally fast and dry west-to-east zonal flow over the western United States. Qualitatively, the no-thunder cases during this final third period of the summer monsoon closely resemble the no-thunder setups during the first third (1 June–10 July), discussed above.

5. Parameter analysis

a. Methodology

In this final section, we consider the gridded surface objective analysis parameters from the SFCOA associated with severe reports for a set of variables related to convective forecasting: 1) mixed layer convective available potential energy (MLCAPE), 2) downdraft convective available potential energy (DCAPE; Gilmore and Wicker 1998), 3) lapse rate in the lowest 3 km above ground level (AGL), and 4) effective bulk wind difference. These variables collectively describe the thermodynamic and kinematic environment of convection across the domain and historically have provided guidance regarding convective intensity in operational forecasting (e.g., Doswell et al. 1982; Schneider and Dean 2008). Given the historical dearth of severe thunderstorm reports in areas outside of urban locations, box-and-whisker plots are provided for an "urban domain," constructed in a manner detailed below. Too few data exist elsewhere for robust samples to statistically substantiate claims regarding severe thunderstorm environments outside of the urban areas.

We define an urban domain as those grid boxes with at least one standard deviation more than the domain-wide

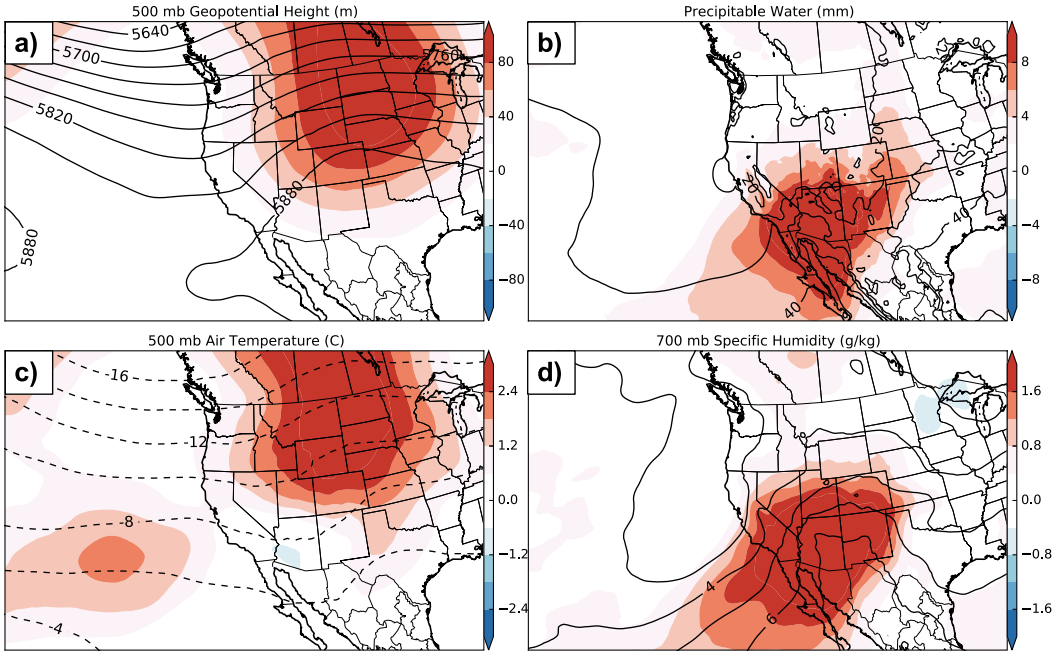

FIG. 12. As in Fig. 10, but for 11 Aug–30 Sep, with $N = 102$.

median number of severe thunderstorm reports (values based on Fig. 5) specifically covering the larger-population Phoenix and Tucson areas. Choosing at least one standard deviation more than the median (two reports) as opposed to the mean (seven reports) is much less restrictive in defining urban grid boxes, thus permitting a wider distribution around the Tucson and Phoenix areas. Ultimately, strictly choosing the median-based threshold also incorporates other locations removed from the Tucson and Phoenix areas (e.g., Yuma), where only isolated grid boxes would contribute to the generation of statistical distributions. However, to focus on more consolidated, contiguous, urban-corridor regimes, we chose to generate statistical distributions from the Tucson and Phoenix area grid boxes only, satisfying the previously mentioned urban domain statistical requirement, as illustrated in Fig. 5.

Within each of the 40-km urban grid points in the SFCOA dataset defined previously, environmental data for a particular hour were recorded as "all severe" if any type of severe weather was reported within the grid box during that hour. This process is then repeated for the individual severe thunderstorm types: wind and hail. The tornado environment is not individually examined in this present study owing to the limited number of tornado reports in our dataset. The environmental dataset for the null cases (i.e., thunderstorms that were not severe) was compiled by recording data in all urban grids with at least one lightning strike during a particular hour on days with no severe weather reported between 1200 and 1159 UTC the following morning. We note that no rigorous statistical tests were performed on these distributions, mainly owing to the large asymmetries in sample sizes, and this is a limitation of this current work. These distributions, however, are meant to provide a direct means to augment a forecaster's contextualization for severe- versus nonsevere-producing environments.

b. Results

Upon grouping all months together during the active monsoon pattern (June–September), Fig. 13 provides an analysis of parameters that could be used to discriminate between severe thunderstorm and nonsevere thunderstorm environments. The largest separation between thunderstorm environments that do not produce severe reports and severe-report-producing environments, dominated by wind reports, is associated with DCAPE. Furthermore, lapse rates in the lowest 3 km AGL are associated with relatively higher 25th and 50th percentiles for severe-wind-producing environments compared to those that do not produce severe reports. This highlights the stronger vertical mixing in the boundary layer in severe-wind-producing environments, which leads to larger downward buoyancy for parcels of air descending from midlevel-initiated downdrafts associated with larger DCAPE. Figure 13 provides the details of these differences and suggests that DCAPE and the low-level lapse rate provide the greatest differences from an operational-forecasting perspective between severe storm and nonsevere storm environments.

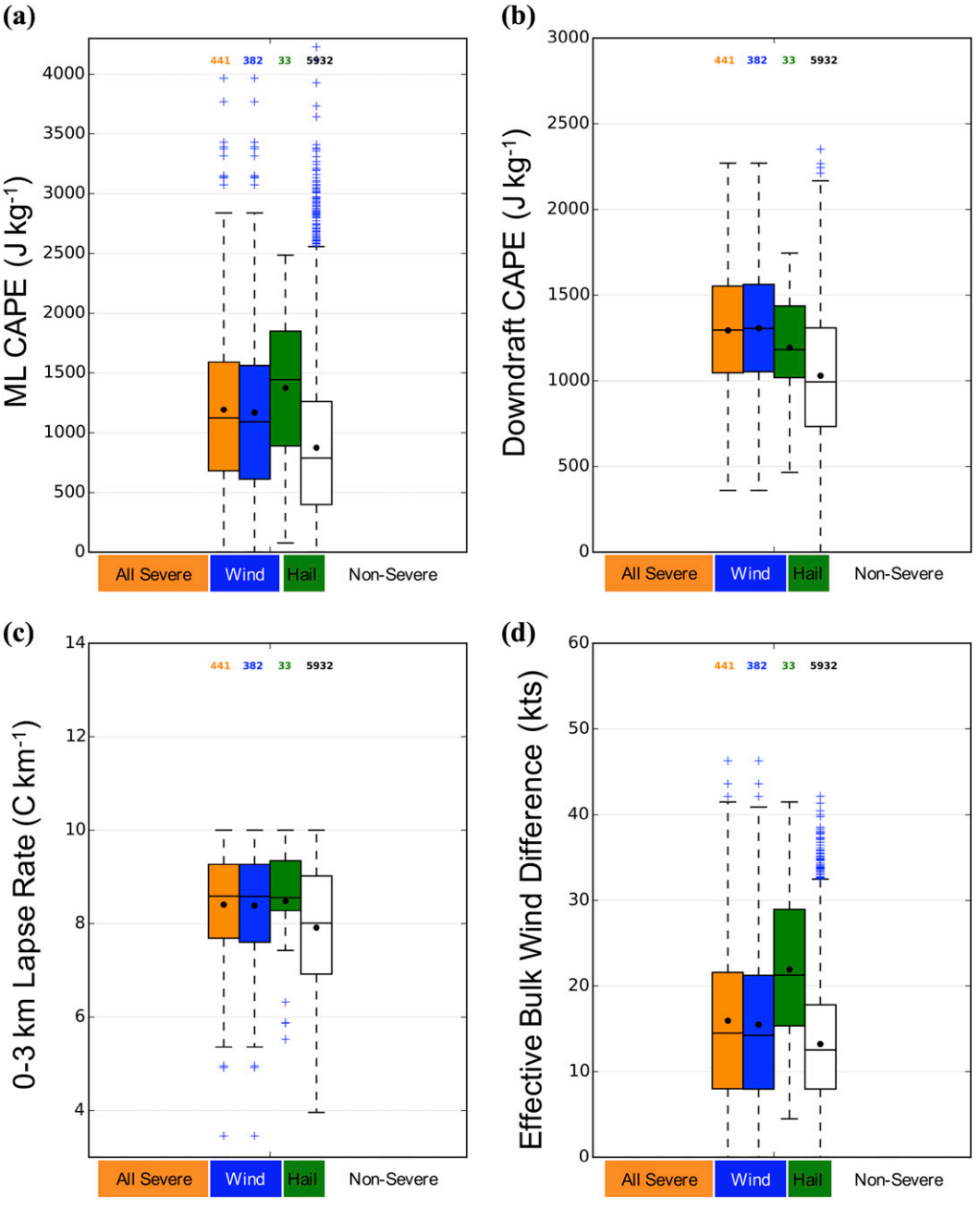

FIG. 13. Box-and-whisker plots of (a) MLCAPE (J kg^{-1}), (b) DCAPE (J kg^{-1}), (c) 0–3-km lapse rate (°C km^{-1}; limited to 10°C km^{-1}), and (d) effective bulk wind difference magnitude (kt) aggregated from June through September and grouped by all severe reports (interquartile range in orange), wind (interquartile range in blue), hail (interquartile range in green), and thunderstorm environments not associated with severe reports (interquartile range in white). The black line is the median value for each box, while the black dot represents the mean of each distribution. The numbers at the top of each plot correspond to the sample size of each distribution.

To assess the influence of deep-layer shear on the propensity for sustained, organized, and potentially severe thunderstorms to occur, we investigate the effective bulk wind difference in Fig. 13. This parameter is similar to the more common 0–6-km bulk wind difference value but is more successful at discriminating among environments favoring storms with varying depths, heights, and equilibrium levels (Thompson et al. 2007). While it was initially developed to aid in the forecasting of supercell thunderstorms, we find some utility in using it to

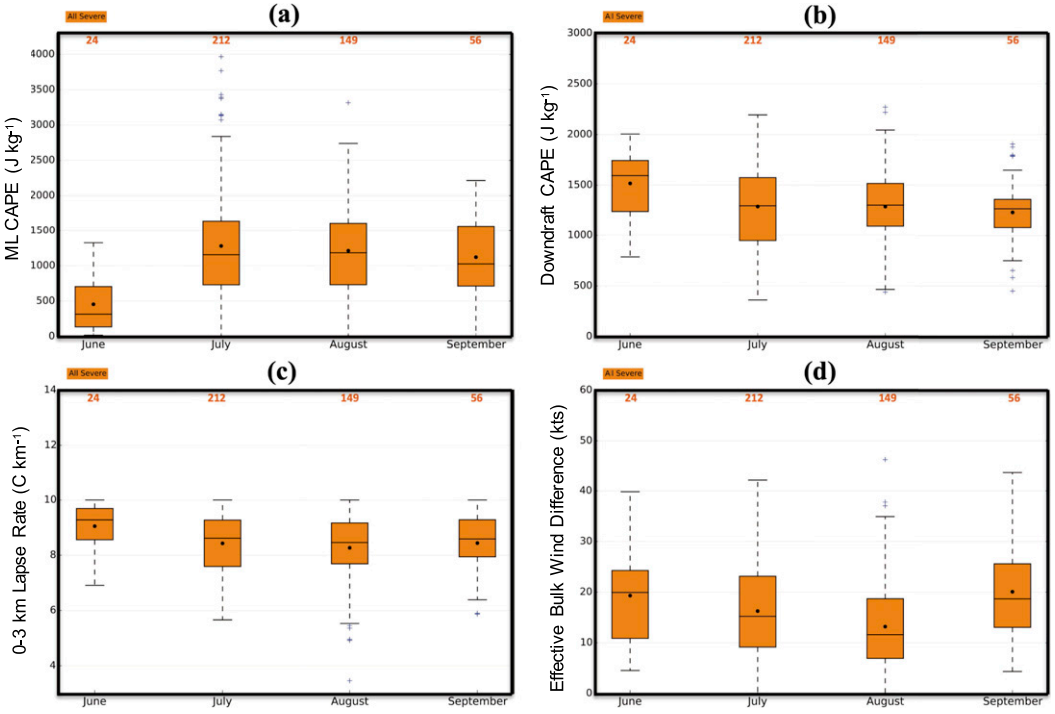

FIG. 14. As in Fig. 13, but separating each month from June through September and combining severe thunderstorm environments (those associated with all severe hazards: wind, hail, and tornadoes) without focus on thunderstorm environments not associated with severe reports.

differentiate between nonsevere thunderstorms and those that produce hail. Substantial separation between the interquartile ranges (25th–75th percentile range) of the hail and nonsevere thunderstorm distributions is noted in Fig. 13, with the hail environments characterized by larger values of effective bulk wind difference, often in excess of 15–20 kt. The typical monsoon environment is characterized by weak midlevel flow owing to the dominance of the mid- and upper-level high that tends to support thunderstorm activity (cf. Figs. 10–12). However, it is clear from Fig. 13 that environments with effective bulk wind difference values favoring the development of multicell or even supercell thunderstorms occasionally develop, which would favor the formation of larger, severe hail (Johns and Doswell 1992).

It is also clear from Fig. 13 that severe and nonsevere thunderstorms occur in environments characterized by a wide range of MLCAPE values, ranging from near $0\,J\,kg^{-1}$ to those exceeding $3000\,J\,kg^{-1}$. In general, the 50th and 75th percentile MLCAPE values for severe thunderstorms tend to be higher than those noted in the nonsevere thunderstorm cases. This is especially evident for severe hail, which can be enhanced by strong updrafts associated with large CAPE.

There is some month-to-month variability regarding thermodynamic and kinematic parameters characterizing severe thunderstorm environments, as illustrated in Fig. 14. MLCAPE values generally increase from June to July and hold nearly steady, with values of $750–1500\,J\,kg^{-1}$ characterizing the middle portion of severe thunderstorm environments. DCAPE decreases slightly through the summer, with values typically exceeding $1000\,J\,kg^{-1}$ throughout the summer. The lapse rate in the 0–3-km layer and effective bulk wind difference are associated with little variability from month to month, with modest amounts of deep shear in severe storm environments (distributions plotted in Fig. 14) and lapse rate values near to slightly below dry adiabatic.

6. Conclusions

This work investigated the synoptic and mesoscale environments associated with convection during the summer monsoon across central and southern Arizona. Using cloud-to-ground lightning strike data from the NLDN, thunderstorm activity was found to peak consistently during the late afternoon hours during the summer monsoon – results that are in agreement with previous work on lightning climatology (King and Balling 1994; Rasmusson 1971; Reap 1986). In addition, late-afternoon peak lightning frequencies were found to focus around higher terrain, where orographic circulations encouraged

thunderstorm development, and lightning frequencies lessened into the early evening. In contrast, some increase in lightning frequencies occurred across the lower elevations into central, south-central, and southwest Arizona from the late-afternoon period into the early evening as convection evolved past the peak of the diurnal heating cycle.

Severe thunderstorm reports were found to be influenced strongly by population distributions, being maximized around the Tucson and Phoenix metropolitan areas during July and August. This signal was more amplified at Phoenix later during the diurnal cycle than at Tucson, suggesting later severe thunderstorm potential climatologically over Phoenix. This notion was further supported by the observation that the temporal distribution of severe weather reports is skewed slightly toward the early to late-evening hours, between 2300 and 0100 UTC, likely the result of initial convection developing over the higher terrain and subsequently advancing toward the valley floors.

We performed a compositing analysis of several pertinent thermodynamic and mass fields in order to construct a climatological timeline of the atmospheric patterns associated with severe weather across the analysis domain using NARR data. In this way, we expand upon earlier work performed by Maddox et al. (1995), which identified three synoptic-scale patterns associated with severe events using coarser reanalysis data and a more limited set of 27 severe weather cases. Our work revealed a variety of patterns conducive to severe thunderstorms across central and southern Arizona, with a clear progression from thunderstorms associated with the subtropical high during the beginning and middle of the summer monsoon to events associated with synoptic-scale troughs as the midlevel high reconsolidates and migrates southward toward the end of the summer.

Finally, guidance was provided to summarize distributions of kinematic and thermodynamic parameters associated with severe thunderstorm reports. Owing to the relative dearth of severe thunderstorm reports outside of the urban Tucson and Phoenix areas, environmental assessment was confined to these areas for severe thunderstorm environments. Greater integrated buoyancy characterized severe-thunderstorm-wind environments than those supporting nonsevere thunderstorms throughout the bulk of the monsoon season. DCAPE and low-level lapse rates were found to offer the best guidance regarding the propensity for storms to produce severe wind gusts, with larger values suggesting deeper vertical mixing and a preconditioned boundary layer for enhancing evaporation in downdrafts and severe wind gusts. Meanwhile, relatively larger effective bulk wind differences, generally over 15–20 kt, were found to typify severe hail environments, reflecting more sustained, organized convection.

Ultimately, this paper provided contextualization of environmental information associated with lightning occurrences and severe thunderstorm occurrences. However, the processes governing aspects such as convective initiation, outflow-related severe storms propagating into the Phoenix area late into the evening and overnight (McCollum 1993), or events characterized by enhanced midlevel flow and a greater occurrence of supercells were not investigated here. Given recent increases in modeling capabilities, this would be interesting follow-up work with great relevance to the operational forecasting community. It is the hope of the authors that this comprehensive analysis and its companion work (Rogers et al. 2017), in which we develop statistical models useful for guidance in evaluating convective potential, will facilitate continued improvements in the understanding of the climatology of Arizona summertime convection, as well as the environments that lead to some of the most impactful weather across the Southwest.

Acknowledgments. NCEP–NCAR reanalysis data were provided by the NOAA/OAR/ESRL/PSD, Boulder, Colorado, from their website (http://www.esrl.noaa.gov/psd). The authors thank Andy Dean of the Storm Prediction Center for providing the SFCOA data used in this study and Dr. Israel Jirak for his assistance in improving this work. We additionally thank the two anonymous reviewers who have greatly improved the readability and the content of this manuscript. Finally, great appreciation is given to the staff at the National Weather Service, Tucson, Arizona, Weather Forecast Office and the Storm Prediction Center for their assistance and input throughout the research process.

REFERENCES

Adams, D. K., and A. C. Comrie, 1997: The North American monsoon. *Bull. Amer. Meteor. Soc.*, **78**, 2197–2213, doi:10.1175/1520-0477(1997)078<2197:TNAM>2.0.CO;2.

Bossert, J. E., and W. R. Cotton, 1994: Regional-scale flows in mountainous terrain. Part I: A numerical and observational comparison. *Mon. Wea. Rev.*, **122**, 1449–1471, doi:10.1175/1520-0493(1994)122<1449:RSFIMT>2.0.CO;2.

Bothwell, P. D., J. A. Hart, and R. L. Thompson, 2002: An integrated three-dimensional objective analysis scheme in use at the Storm Prediction Center. Preprints, *21st Conf. on Severe Local Storms/19th Conf. on Weather Analysis and Forecasting/15th Conf. on Numerical Weather Prediction*, San Antonio, TX, Amer. Meteor. Soc., J117–J120. [Available online at https://ams.confex.com/ams/pdfpapers/47482.pdf.]

——, B. T. Smith, R. L. Thompson, A. R. Dean, and J. S. Kain, 2014: Severe weather parameter reanalysis project at the Storm Prediction Center. Preprints, *27th Conf. on Severe*

Local Storms, Madison, WI, Amer. Meteor. Soc., 18.2. [Available online at https://ams.confex.com/ams/27SLS/webprogram/Paper255652.html.]

Bryson, R. A., and W. P. Lowry, 1955: The synoptic climatology of the Arizona summer precipitation singularity. *Bull. Amer. Meteor. Soc.*, **36**, 329–339.

Carleton, A. M., 1986: Synoptic-dynamic character of 'bursts' and 'breaks' in the south-west U.S. summer precipitation singularity. *J. Climatol.*, **6**, 605–623, doi:10.1002/joc.3370060604.

Cummins, K. L., and M. J. Murphy, 2009: An overview of lightning locating systems: History, techniques, and data uses, with an in-depth look at the U.S. NLDN. *IEEE Trans. Electromagn. Compat.*, **51**, 499–518, doi:10.1109/TEMC.2009.2023450.

Doran, J. C., and S. Zhong, 1994: Regional drainage winds in the Pacific Northwest. *Mon. Wea. Rev.*, **122**, 1158–1167, doi:10.1175/1520-0493(1994)122<1158:RDFITP>2.0.CO;2.

Doswell, C. A., III, J. T. Schaefer, and D. W. McCann, 1982: Thermodynamic analysis procedures at the National Severe Storms Forecast Center. Preprints, *Ninth Conf. on Weather Forecasting and Analysis*, Seattle, WA, Amer. Meteor. Soc., 304–309.

Douglas, M. W., R. A. Maddox, J. Howard, and S. Reyes, 1993: The Mexican monsoon. *J. Climate*, **6**, 1665–1677, doi:10.1175/1520-0442(1993)006<1665:TMM>2.0.CO;2.

Gilmore, M. S., and L. J. Wicker, 1998: The influence of midtropospheric dryness on supercell morphology and evolution. *Mon. Wea. Rev.*, **126**, 943–958, doi:10.1175/1520-0493(1998)126<0943:TIOMDO>2.0.CO;2.

Glueck, J. R., 1997: Climate of Tucson, Arizona. NOAA Tech. Memo. NWS WR-249, 121 pp. [Available online at https://www.weather.gov/media/wrh/online_publications/TMs/TM-249.pdf.]

Green, C. R., and W. S. Sellers, 1964: *Arizona Climate.* University of Arizona Press, 503 pp.

Hales, J. E., Jr., 1974: Southwestern United States summer monsoon source—Gulf of Mexico or Pacific Ocean? *J. Appl. Meteor.*, **13**, 331–342, doi:10.1175/1520-0450(1974)013<0331:SUSSMS>2.0.CO;2.

——, 1977: On the relationship of convective cooling to nocturnal thunderstorms at Phoenix. *Mon. Wea. Rev.*, **105**, 1609–1613, doi:10.1175/1520-0493(1977)105<1609:OTROCC>2.0.CO;2.

Hart, J. A., and W. D. Korotky, 1991: The SHARP workstation v1.50: User's guide. NOAA/NWS, 30 pp.

Johns, R. H., and C. A. Doswell III, 1992: Severe local storms forecasting. *Wea. Forecasting*, **7**, 588–612, doi:10.1175/1520-0434(1992)007<0588:SLSF>2.0.CO;2.

King, T. S., and R. C. Balling Jr., 1994: Diurnal variations in Arizona monsoon lightning data. *Mon. Wea. Rev.*, **122**, 1659–1664, doi:10.1175/1520-0493(1994)122<1659:DVIAML>2.0.CO;2.

Lopez, R. E., and R. L. Holle, 1986: Diurnal and spatial variability of lightning activity in northeastern Colorado and central Florida during the summer. *Mon. Wea. Rev.*, **114**, 1288–1312, doi:10.1175/1520-0493(1986)114<1288:DASVOL>2.0.CO;2.

Maddox, R. A., M. Douglas, and K. W. Howard, 1991: Mesoscale precipitation systems over southwestern North America: A warm season overview. Preprints, *Int. Conf. on Mesoscale Meteorology and TAMEX*, Taipei, Taiwan, Amer. Meteor. Soc. and NCAR, 393–402.

——, D. McCollum, and K. Howard, 1995: Large-scale patterns associated with severe summertime thunderstorms over central Arizona. *Wea. Forecasting*, **10**, 763–778, doi:10.1175/1520-0434(1995)010<0763:LSPAWS>2.0.CO;2.

McCollum, D. M., 1993: Synoptic-scale patterns associated with severe thunderstorms in Arizona during the summer monsoon. M.S. thesis, School of Meteorology, University of Oklahoma, 166 pp.

Mesinger, F., and Coauthors, 2006: North American Regional Reanalysis. *Bull. Amer. Meteor. Soc.*, **87**, 343–360, doi:10.1175/BAMS-87-3-343.

Rasmusson, E. M., 1967: Atmospheric water vapor transport and the water balance of North America: Part I. Characteristics of the water vapor flux field. *Mon. Wea. Rev.*, **95**, 403–426, doi:10.1175/1520-0493(1967)095<0403:AWVTAT>2.3.CO;2.

——, 1971: Diurnal variation of summertime thunderstorm activity over the United States. Tech. Note 71-4, USAF Environmental Technical Applications Center, 13 pp.

Reap, R., 1986: Evaluation of cloud-to-ground lightning from the western United States for the 1983–84 summer seasons. *J. Appl. Meteor.*, **25**, 785–799, doi:10.1175/1520-0450(1986)025<0785:EOCTGL>2.0.CO;2.

Reitan, C. H., 1957: The role of PW vapor in Arizona's summer rains. Meteorology and Climatology of Arid Regions Tech. Rep. 2, Institute of Atmospheric Physics, The University of Arizona, Tucson, AZ, 18 pp.

Rogers, J. W., A. E. Cohen, and L. B. Carlaw, 2017: Convection during the North American monsoon across central and southern Arizona: Applications to operational meteorology. *Wea. Forecasting*, 32, 377–390, doi:10.1175/WAF-D-15-0097.1.

Schneider, R. S., and A. R. Dean, 2008: A comprehensive 5-year severe storm environment climatology for the continental United States. Preprints, *24th Conf. on Severe Local Storms*, Savannah, GA, Amer. Meteor. Soc., 16A.4. [Available online at https://ams.confex.com/ams/24SLS/techprogram/paper_141748.htm.]

Sellers, W. W., and R. H. Hill, 1974: *Arizona Climate: 1931–1972.* University of Arizona Press, 616 pp.

Shoemaker, C., and J. T. Davis, 2008: Hazardous weather climatology for Arizona. NOAA Tech. Memo. NWS-WR 282, 47 pp. [Available online at http://www.wrh.noaa.gov/wrh/techMemos/TM-282.pdf.]

Smith, B. T., T. E. Castellanos, A. C. Winters, C. M. Mead, A. R. Dean, and R. L. Thompson, 2013: Measured severe convective wind climatology and associated convective modes of thunderstorms in the contiguous United States. *Wea. Forecasting*, **28**, 229–236, doi:10.1175/WAF-D-12-00096.1.

Tang, M., and E. R. Reiter, 1984: Plateau monsoons of the Northern Hemisphere: A comparison between North America and Tibet. *Mon. Wea. Rev.*, **112**, 617–637, doi:10.1175/1520-0493(1984)112<0617:PMOTNH>2.0.CO;2.

Thompson, R. L., C. M. Mead, and R. Edwards, 2007: Effective storm-relative helicity and bulk shear in supercell thunderstorm environments. *Wea. Forecasting*, **22**, 102–115, doi:10.1175/WAF969.1.

Toth, J. J., and R. H. Johnson, 1985: Summer surface flow characteristics over northeast Colorado. *Mon. Wea. Rev.*, **113**, 1458–1469, doi:10.1175/1520-0493(1985)113<1458:SSFCON>2.0.CO;2.

Vasiloff, S. V., and K. W. Howard, 2009: Investigation of a severe downburst storm near Phoenix, Arizona, as seen by a mobile Doppler radar and the KIWA WSR-88D. *Wea. Forecasting*, **24**, 856–867, doi:10.1175/2008WAF2222117.1.